Available online at www.sciencedirect.com
ScienceDirect
Journal of Power Sources 161 (2006) 11–18
JOURNAL OF POWER SOURCES
www.elsevier.com/locate/jpowsour

Effect of dispersion methods of an unsupported Pt-Ru black anode catalyst on the power performance of a direct methanol fuel cell

Chan Lim [a,*], R.G. Allen [b], K. Scott [b]

[a] *R&D Center, Dymos Inc., Hyundai Motor Group, KyungKi-Do 463-728, Republic of Korea*
[b] *School of Chemical Engineering and Advanced Materials, University of Newcastle upon Tyne, Newcastle upon Tyne NE1 7RU, United Kingdom*

Received 1 November 2005; received in revised form 20 February 2006; accepted 24 February 2006
Available online 23 May 2006

Abstract

The effect of the dispersion methods for an unsupported Pt-Ru (1:1) black anode catalyst on the power performance of a direct methanol fuel cell has been studied. The anode catalyst inks were fabricated by ultrasonicating or ball-milling the catalyst in two different types of dispersion solvent, namely deionized water (DI) and isopropyl alcohol (IPA). To fabricate an anode, the inks were sprayed onto the gas diffusion backing electrode, consisting of microporous layer (MPL) and carbon paper. Scanning electron microscopy (SEM) of the cross-sectional morphology of the anode catalyst layers revealed that the layers fabricated by ultrasonicating the catalyst in DI or IPA, ball-milling in DI and ball-milling in IPA consisted of granular-shaped, granular + flake-shaped and flake-shaped agglomerates, respectively. The anode catalyst layer fabricated by ball-milling in IPA exhibited the most porous structure and correspondingly represented the best power performance of 0.13 W cm^{-2} (0.45 A cm^{-2}, 0.3 V) at 90 °C with 1 M aqueous methanol and atmospheric air. Control of the morphology and porosity in the catalyst layer by means of the catalyst dispersion method is suggested.

Keywords: Direct methanol fuel cell; Unsupported Pt-Ru; Dispersion; Catalyst layer; Porosity; Ball-mill

1. Introduction

A liquid-feed direct methanol fuel cell (DMFC) based on a Nafion proton exchange membrane (PEM) has attracted much interest due to its simplicity in system design, e.g., no need for hydrogen storage or a fuel reformer, or humidification of the hydrogen and air. However, direct methanol fuel cells have demonstrated much lower peak power density than H_2-fueled PEMFC because methanol oxidation kinetics in the anode catalyst are sluggish, leading to a relatively large loss in cell voltage. The cell voltage is further lowered by methanol permeating through the membrane toward the cathode.

Although the catalyst loadings have been quite high, e.g., above 2 mg cm^{-2}, the power output using an unsupported Pt-Ru catalyst in the anode have been reported to be higher than using a carbon supported Pt-Ru [1–6]. It has been shown, as a result of simulation studies in a methanol/air polymer electrolyte fuel cell [7], that high concentrations of CO_2 are encountered deep inside the catalyst layer and can induce mass transport limitations. The unsupported catalyst seems to mitigate the CO_2 transport problem because the catalyst layer is much thinner using the unsupported catalyst than using the carbon supported catalyst with a similar catalyst loading. Significant efforts have been made to synthesize unsupported PtRu alloy catalysts that are as fine as possible to find optimum compositions of the catalyst for electrochemical methanol oxidation [3,5,8]. Recently, there have been a few studies on how dispersion methods [9] and dispersion solvents [10] for processing the nanocatalyst affect the morphology of the resulting catalyst layer and therefore the polarization behaviour of the electrode towards the methanol oxidation reaction. It is believed an understanding of the phenomena during the ink processing of the catalyst might be important to increasing utilization of the catalyst layer in combination with compositional controls of the catalyst and catalyst layer.

The objective of this study is to survey morphological changes in the catalyst layer and to increase the power output of DMFC-MEA by using different types of dispersion methods and

* Corresponding author. Tel.: +82 31 728 1480; fax: +82 31 728 1466.
E-mail address: to-chan-lim@hanmail.net (C. Lim).

0378-7753/$ – see front matter © 2006 Elsevier B.V. All rights reserved.
doi:10.1016/j.jpowsour.2006.02.101

dispersion media with a commercial unsupported Pt-Ru black anode catalyst based upon Nafion 117.

2. Experimental

In this study, a spray-coating technique was used to fabricate both the anode and cathode catalyst layers on microporous layer-coated gas diffusion backing electrodes. A paste for the microporous layer was formulated by dispersing Vulcan XC72R (Cabot) carbon black and Teflon (33 wt.% emulsion, Fluon) into a water and alcohol mixture, and was spread on a commercial 20 wt.% wet-proofed carbon paper (Toray 090, E-Tek) by a gap-adjustable knife-blade (Sheen Instruments), followed by drying at 100 °C and sintering at 360 °C in atmospheric air for 30 min.

Four different inks for the anode catalyst layer were prepared by dispersing unsupported Pt-Ru black (HiSPEC 6000, Pt:Ru = 1:1 atomic ratio, Alfa Aesar) and 20 wt.% (in catalyst layer) of Nafion solution (5 wt.% Nafion solution, EW: 1100, Aldrich Chemical) into de-ionized water (DI) or isopropyl alcohol (IPA) by using ultrasonication or ball-milling methods, as summarized in Table 1. The ultrasonication was done for 1 h and the ball-milling process was done for 2 h after inserting zirconia beads (diameter 3 mm) into a glass bottle of the catalyst layer ink in a volume ratio of ball to ink 1:3 and subjecting it in a flask shaker (Stuart Scientific, Inc.). The inks were applied onto the microporous layer-coated gas diffusion backing electrode by using a spray gun (Model 100 LG, Badger), followed by drying at 80 °C for 30 min in an atmospheric air oven. In working with the DI-based ink, the GDL substrate was heated up to 80 °C during the spray-coating process due to the low volatility of DI, facilitating evaporation of the solvent in droplets of the ink. The amount of Pt-Ru catalyst loading was controlled to be 2 mg cm^{-2} (total weight of Pt and Ru per geometric area of electrode). An ink for the cathode catalyst layer was consistently made by dispersing Pt supported on carbon (60 wt.% Pt on Vulcan XC72, E-Tek) and 30 wt.% (in catalyst layer) of Nafion solution into isopropyl alcohol by ball-milling for 2 h, followed by the same procedure as that of the anode. The amount of Pt loading was controlled to be 4.5 mg cm^{-2}.

A Nafion 117 membrane (EW 1100, Dupont) was preliminarily subjected to a cleaning procedure. After trimming the catalyzed electrodes for the anode and cathode respectively, these were positioned on both sides of the pre-cleaned membrane and hot-pressed to form a MEA at 125 °C and 70 kg cm^{-2} for 3 min. The MEA was installed into a single cell fixture (consisting of graphite plates with an active area of 9 cm^2) having straight parallel flow channels with a width of 1.5 mm, a depth of 2 mm and a rib width of 0.5 mm for both the anode and cathode. A dilute methanol solution was fed to anode inlet at a flow rate of 12 cm^3 min^{-1} by a peristaltic pump (101U/R, Watson) without pre-heating and back-pressurization. Non-humidified, room temperature air was fed to the cathode inlet at a flow rate of 1 dm^3 min^{-1} without pre-heating and back-pressurization. Polarization curves were obtained after voltages were stabilized for at least 10 min after onset of galvanostatic currents. The anode polarization behaviour, including the ohmic voltage drops through the electrodes and the membrane, was measured in the single cell hardware with respect to a hydrogen-evolving cathode acting as a dynamic hydrogen electrode (DHE).

X-ray diffraction data for the anode catalyst powder and electrode were obtained using Philips Xpert Pro diffractometer operating at 40 kV accelerating voltage and 40 mA of beam current, and using Cu Kα1 radiation. Analysis of the XRD data was carried out using Philips Xpert High Score. The surface and cross-sectional morphologies of the anode catalyst layers were surveyed by a JEOL 6300 scanning electron microscope (SEM), equipped with computerized digital image software. The particle size distribution was obtained from the catalyst layer inks by Malvern Master Sizer 2000 using laser beam scattering method.

CO-stripping voltammetry was performed in a three-electrode jacketed glass cell, using an MMS reference electrode (0.64 V versus RHE) and a Pt mesh counter electrode. All electrode potentials throughout this paper are referred to the RHE scale. The working electrode was enveloped in a titanium mesh current collector, which showed negligible contribution of current to the voltammetry. The cell temperature was maintained at 60 °C during the experiment. The potential was scanned at 5 mV s^{-1} by using an EG&G Model 363 Scanning Potentiostat and Sycopel Scientific software Version 3.60 for data collection. The dry electrode sample was placed in an N_2-purged and N_2-blanketed cell at 60 °C and was subsequently cycled between −0.06 and 0.66 V_{RHE} at 5 mV s^{-1} every 30 min until a stable voltammogram was obtained. Following this hydration period, CO was adsorbed on the electrode surface at 0.04 V_{RHE} by bubbling CO gas through the 0.5 M H_2SO_4 solution for 1 h. The CO, which was dissolved in the electrolyte, was subsequently removed by bubbling N_2 throughout the electrolyte for 30 min. The solution was stirred with a magnetic bar during both the CO-adsorption and the N_2-purging periods to increase the distribution of gas. The potential was then scanned at 5 mV s^{-1} in the anodic direction from the holding potential. The peak area of CO oxidation, taking place in the first cycle, was obtained by integrating the current density versus time in order to evaluate the charge and then active area of the anodes.

Table 1
Preparation methods of inks using two different dispersion solvents and two different dispersion methods for the anode

Sample classification	Main composition	Dispersion solvent	Dispersion method
Ultrasonication-processed in DI	Pt-Ru black: 1 g, Nafion solution: 5 g	DI: 104.4 g	Ultrasonication for 1 h
Ball-mill-processed in DI	Pt-Ru black: 1 g, Nafion solution: 5 g	DI: 104.4 g	Ball-milling for 2 h
Ultrasonication-processed in IPA	Pt-Ru black: 1 g, Nafion solution: 5 g	IPA: 79.1 g	Ultrasonication for 1 h
Ball-mill-processed in IPA	Pt-Ru black: 1 g, Nafion solution: 5 g	IPA: 79.1 g	Ball-milling for 2 h

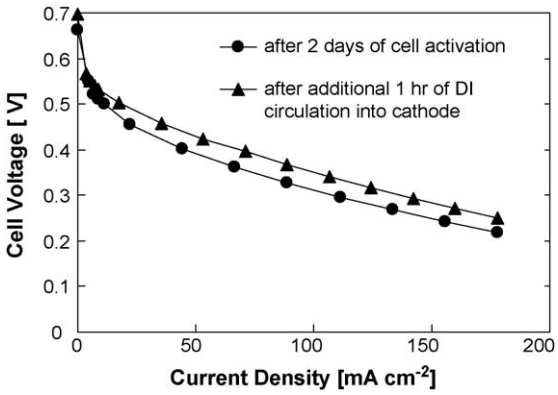

Fig. 1. Effect of the activation method of a single cell on the polarization behaviour of the MEA measured at 90 °C in 2 M CH_3OH; anode catalyst layer: 2 mg cm^{-2} of unsupported Pt-Ru; cathode catalyst layer: 4.5 mg cm^{-2} of 60 wt.% Pt/C.

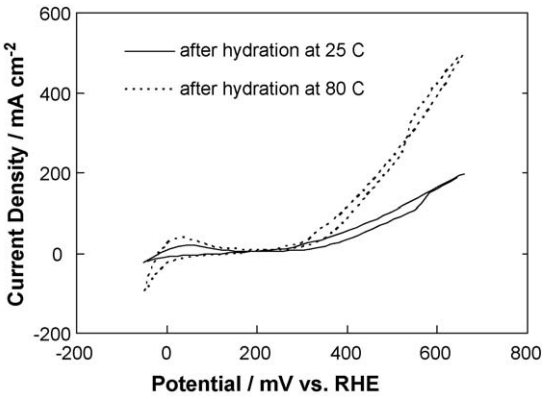

Fig. 2. Effect of pre-treatment hydration on the cyclic voltammogram of an anode electrode obtained at 60 °C and a scan rate of 20 mV s^{-1} in 0.5 M H_2SO_4 + 2 M CH_3OH; catalyst layer: 2 mg cm^{-2} of Pt-Ru black and 20 wt.% Nafion.

3. Results and discussion

To evaluate the polarization characteristics of the membrane electrode assemblies, it is essential to obtain an activation procedure that ensures a steady-state and reproducible power output. The effect of the activation methods on the single cell power performance of DMFC-MEA is demonstrated in Fig. 1. A general method of DMFC cell activation has been by circulating 1 mol m^{-3} (M) aqueous methanol through the anode compartment of the single cell at 90 °C for at least 24 h [11,12]. Even though the MEA was conditioned for 2 days by circulating aqueous methanol through the anodic compartment of the cell, it did not approach a steady-state polarization curve representing the characteristics of the MEA. After circulating de-ionized water into the cathode compartment additionally for 1 h, the MEA showed higher performance and more reproducible polarization curve. Hereafter, we consistently carried out a standard procedure of DMFC single cell activation in which 1 M aqueous methanol and de-ionized water were circulated for 12 h through the anodic and the cathodic compartment of the single cell, respectively, whenever a fresh MEA was installed into the single cell fixture. After that, the MEA was conditioned for 10 min at the cell voltage of 0.3 V in order to establish an equilibrium state at the experimental operating condition.

To understand the importance of hydration in the fuel cell electrode, cyclic voltammetry was carried out on an electrode sample before and after fully hydrating by immersion in de-ionized water at 80 °C, and the results are shown in Fig. 2. As the sample was fully hydrated in hot water, the hydrogen desorption charge increased from 64 to 121 mQ cm^{-2} and correspondingly the methanol oxidation kinetic current density markedly increased, indicating that more catalytic sites become available for electrochemical charge transfer reactions as a result of the hydration of the electrode. From the water uptake experiments of Nafion 117 membrane, Zawodzinski et al. [13] reported that the membrane, once dried at an elevated temperature of 105 °C, showed a lower water uptake upon rehydration than the one dried at room temperature, and that the amount of water uptake in the membrane dried at the elevated temperature increased with the rehydration temperature. As the proton conductivity in the Nafion membrane linearly increases with water content in the membrane, it can be explained that the catalyst layer subjected to rehydration at a higher temperature would have higher proton conductivity and therefore achieve higher catalyst utilization, as shown in Fig. 2. In these reasons, the new activation procedure that circulates the methanol solution and the de-ionized water through the anodic and the cathodic compartment, respectively, would effectively hydrate both electrodes and enables a reliable evaluation of the power performance of MEA for the DMFC.

To survey the crystallographic changes in Pt-Ru black as a result of three different dispersion methods of anode catalyst, X-ray diffraction (XRD) patterns were taken from an as-received sample of Pt-Ru black and three different fuel cell anodes from the inks prepared by ultrasonication in de-ionized water, ball-milling in de-ionized water and ball-milling in isopropyl alcohol, respectively, and are presented in Fig. 3. The as-received Pt-Ru back exhibited very similar XRD patterns to those obtained by Dinh et al. [14] representing a typical face-centered cubic (fcc) structure consisting of PtRu bimetallic alloy. The XRD patterns taken from the fuel cell electrode involved (0 0 2) and (0 0 4) peaks at interspacing distances d of 0.34 and 0.17 nm,

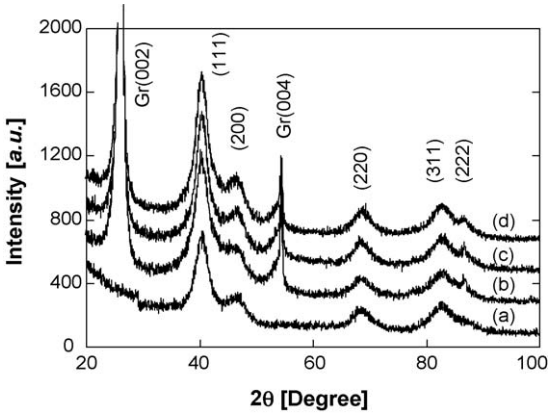

Fig. 3. XRD patterns of: (a) as-received Pt-Ru black, (b) anode fabricated by ultrasonication in DI, (c) anode fabricated by ball-milling in de-ionized water and (d) anode fabricated by ball-milling in IPA.

Table 2
Mean particle size and metal surface area of the anode samples calculated from XRD patterns in Fig. 3

Sample classification	Mean particle size, Å (±2 Å)	Metal surface area* ($m^2\ g^{-1}$)
As-received Pt-Ru black	38	98
Ultrasonication-processed in DI	45	78
Ball-mill-processed in DI	50	70
Ball-mill-processed in IPA	44	80

* Calculated from XRD data assuming spherical particle and density of 17 $g\ cm^{-3}$ [14].

respectively, resulting from the highly graphitized carbon paper backing electrodes. Comparing the XRD patterns from the as-received Pt-Ru black and the fuel cell electrodes, there was no appreciable shift in the *d*-spacings of (1 1 1), (2 2 0) and (3 1 1) planes, indicating that there is no change in lattice parameter and correspondingly bulk composition of PtRu bimetallic alloy catalysts.

As the anode catalyst powder is processed to the anode catalyst layer via the dispersion/drying procedure, the XRD patterns from all electrode samples presented a (2 2 2) peak which was not explicitly observed in the as-received powder sample. Therefore, it is believed that the catalyst particles in the catalyst layer have a more crystallographically ordered structure than those in the as-received powder, probably originating from agglomerations during the catalyst layer fabrication process. The mean particle sizes in all samples were estimated from the line-broadening of the (2 2 0) peaks using the Scherrer formula [15,16] and are summarized in Table 2, including the metal surface area calculated from the XRD mean particle size [5]. The mean particle size was evaluated to be slightly bigger in the fuel cell electrodes than in the as-received Pt-Ru black powder, also indicating the beneficial effect of agglomeration of catalyst particles during catalyst layer fabrication process. However, it is noticed that the estimation of particle size using the XRD pattern might not be so sensitive to the particle agglomeration because the method reflects only the changes in the size of component crystallite in the original unsupported Pt-Ru black particles and the dispersion methods in this study might not have enough energy to induce changes the size of the crystallite in the unsupported Pt-Ru particles.

Particle size distribution was measured by using laser diffraction method from catalyst layer inks prepared by the ultrasonication and ball-milling methods in DI and IPA, and the results are shown in Fig. 4. First of all, two main peaks were observed in the particle size distribution, i.e., one (P1) in the region 0.03–1 μm and another one (P2) in the region 1–30 μm. Kim et al. [10] studied changes in size distribution of perfluoro-sulfonated ionomer (PFSI) agglomerates using the laser light scattering method and observed changes in a peak position in the region 0.04–2 μm, which corresponds to the particle size region of the peak P1 in this study. Therefore, it is suggested that the peak P1 comes from distributed sizes of PFSI agglomerates in the dispersion solvent. Subsequently, the peak P2 is reasonably assigned to a size distribution of catalyst particle agglomerates, based on the result [9] that measured size distributions of carbon black catalyst supporter in the region 0.4–20 μm depending on nano-particle dispersion methods using the same light diffraction method.

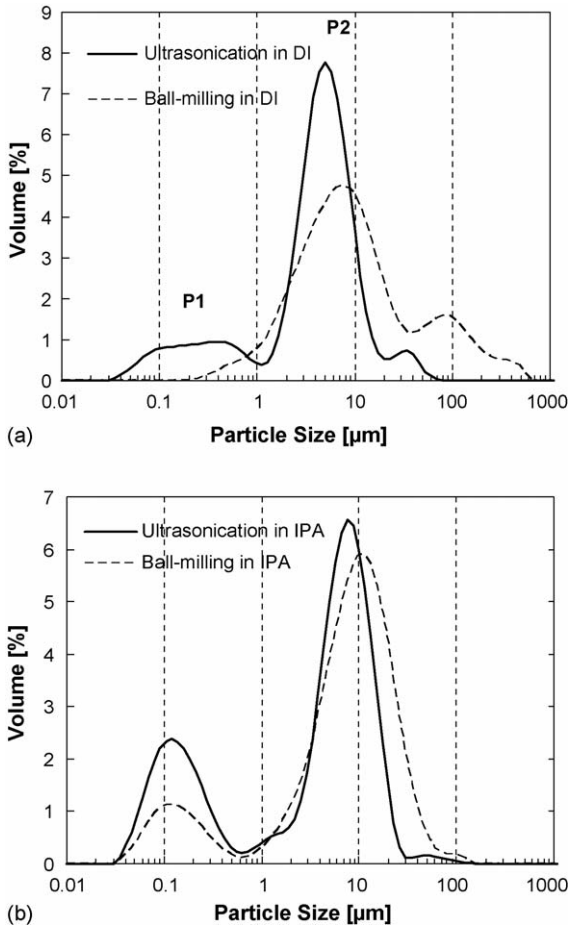

Fig. 4. Particle size distribution in inks prepared by different dispersion methods in different dispersion media: (a) de-ionized water; (b) isopropyl alcohol.

In Fig. 4(a), the ball-milling process in the DI dispersion media explicitly made the catalyst particles form agglomerates bigger than those processed with ultrasonication, due to vigorous mechanical collisions between the nano-particles in the solvent provided by the ball-milling process. It is noteworthy that the peak intensity of P1 in the ink processed with ultrasonication in DI as shown in Fig. 4(a) was observed to be much lower than that in the IPA-based ink shown in Fig. 4(b). Furthermore, the peak P1 disappeared as a result of the ball-milling process in DI. Uchida et al. [17] suggested that PFSI ionomer particles tend to precipitate in solvents having a low dielectric constant ($\varepsilon < 3$), and become colloidal in solvents ($3 < \varepsilon < 10$) and dissolve in solvents ($\varepsilon > 10$). Considering the high dielectric constant ($\varepsilon = 78.5$) of DI, the PFSI particles seem to dissolve into the DI solvent as a result of the ball-milling agitation as shown in Fig. 4(a). Contrary to the result [9] that a ball-milling process made carbon-supported catalyst agglomerate less, it forced the unsupported Pt-Ru catalyst agglomerates to be bigger due to the face-centered cubic structure of Pt-Ru being susceptible to plastic deformation upon mechanical impacts.

To survey the macroscopic changes in the morphology of the catalyst layer with the dispersion methods of Pt-Ru black,

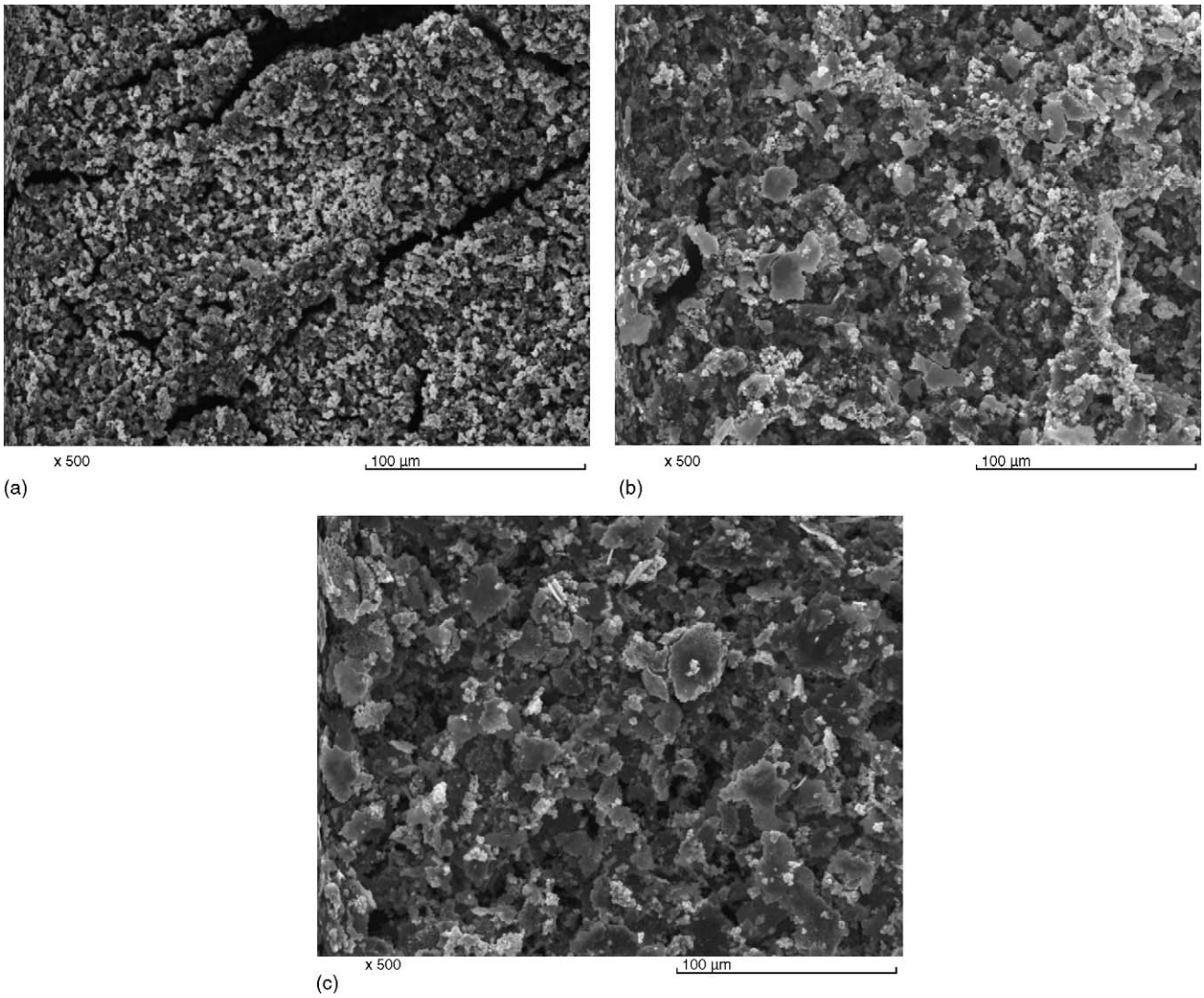

Fig. 5. Surface view of SEM micrographs of anodes prepared by spray-coating from different inks: (a) processed by ultrasonication in isopropyl alcohol or de-ionized water, (b) processed by ball-milling in de-ionized water and (c) processed by ball-milling in isopropyl alcohol; catalyst layer: 2 mg cm^{-2} of Pt-Ru black and 20 wt.% Nafion.

the surface and the cross-sectional surface of the sample electrodes were examined by scanning electron microscopy and the results are shown in Figs. 5 and 6, respectively. From the surface view of SEM micrograph in Fig. 5(a), the catalyst layers prepared by the ultrasonication method in IPA or DI both showed identical surface morphologies, consisting of granular-shaped particulates from several to 5 μm in diameter corresponding with the result from the particle size distribution measurements. The anode catalyst layers fabricated by ultrasonicating the catalyst powder in IPA or DI appear to be 10–15 μm thick in the cross-sectional view of SEM micrograph presented in Fig. 6(a). Fig. 5(b) represents a surface morphology of the anode catalyst layer, fabricated by ball-milling the catalyst powder in DI, consisting of the granular particles and additionally flake-shaped particles having a diameter range of 5–30 μm and a thickness less than 3 μm. The thickness of the catalyst layer was evaluated to be about 25 μm in Fig. 6(b). Finally, in Figs. 5 and 6(c), the anode catalyst layer fabricated by ball-milling the catalyst powder in IPA showed a morphology consisting of the flake-shaped particles only, having a thickness about 25 μm. It is clearly observed that the mechanical dispersion method, i.e., ball-milling process, forced the catalyst powder to agglomerate, partially by fusing and forming flake-shaped particles.

Fig. 7 shows the effect of the catalyst dispersion method on the polarization curve of the MEA, obtained at 90 °C in 1 M aqueous methanol as an anode fuel and atmospheric pressure air as a cathode oxidant after subjecting the MEA to our new activation procedure mentioned before. The MEAs with the anodes processed in IPA as a dispersion media showed much higher power performance than those processed in DI. First of all, this can result from the status of PFSI dissolved in the DI-based ink as evident in Fig. 4(a), which leads to a thinner PFSI film on the catalyst particles in the catalyst layer and hence decreased proton conductivity through the porous structure in the catalyst layer, representing a lower utilization of the catalyst particles. A similar result [10] has been reported when methanol ($\varepsilon = 33.1$) was used as a dispersion solvent in comparison to using dipropyl ketone ($\varepsilon = 12.6$) or *n*-butyl acetate ($\varepsilon = 5.0$). Secondly, the low

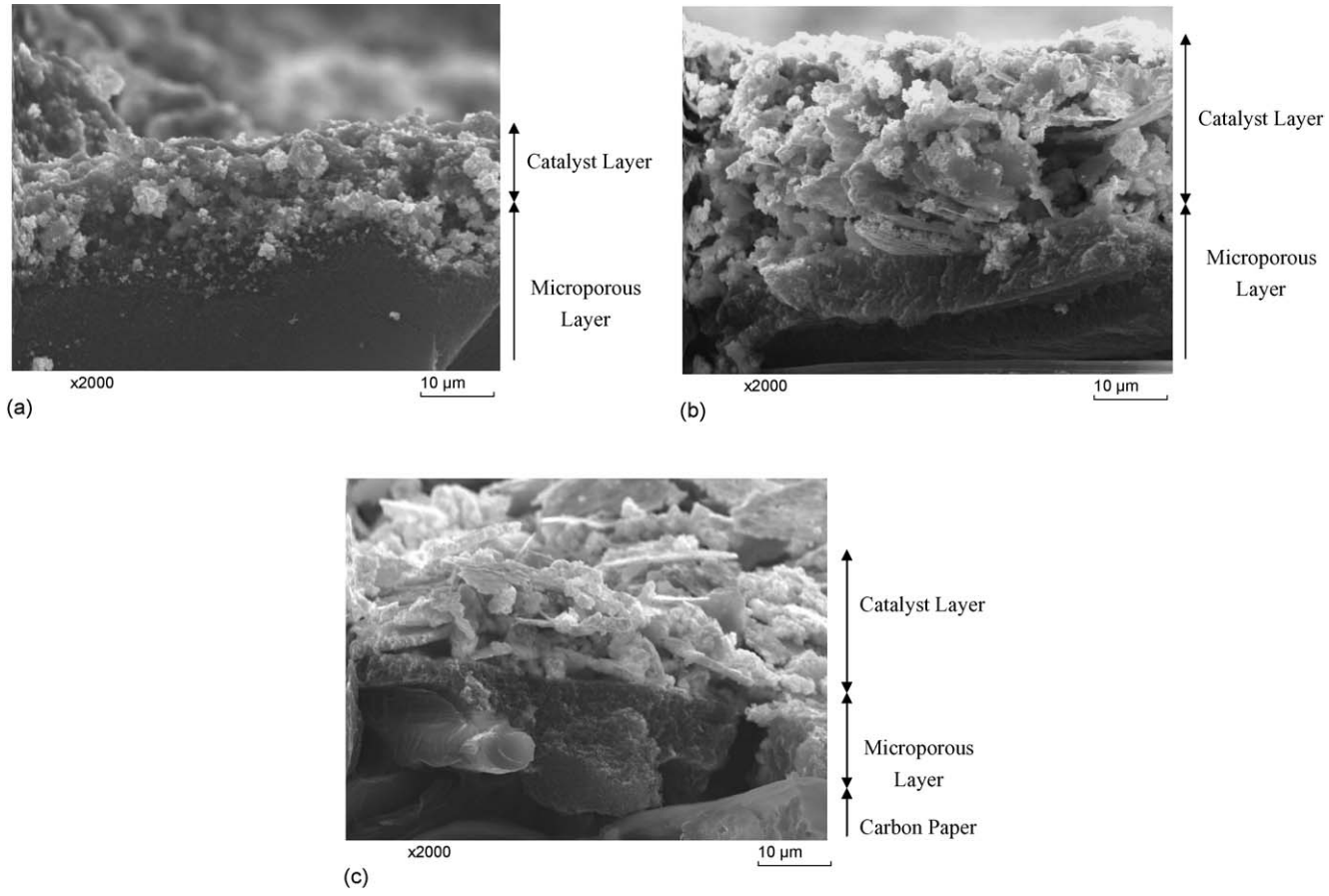

Fig. 6. Cross-sectional SEM micrographs of anodes prepared by spray-coating from different inks: (a) processed by ultrasonication in isopropyl alcohol or de-ionized water, (b) processed by ball-milling in de-ionized water and (c) processed by ball-milling in isopropyl alcohol; catalyst layer: 2 mg cm^{-2} of Pt-Ru black and 20 wt.% Nafion.

performance of the anode using DI-based ink might be due to the high polarity of water molecules. The high hydrophobicity of the MPL toward the DI solvent might not allow the ink to penetrate its surface and hence decrease the integrity between the catalyst layer and the MPL, resulting in a high interfacial ohmic resistance at the interface.

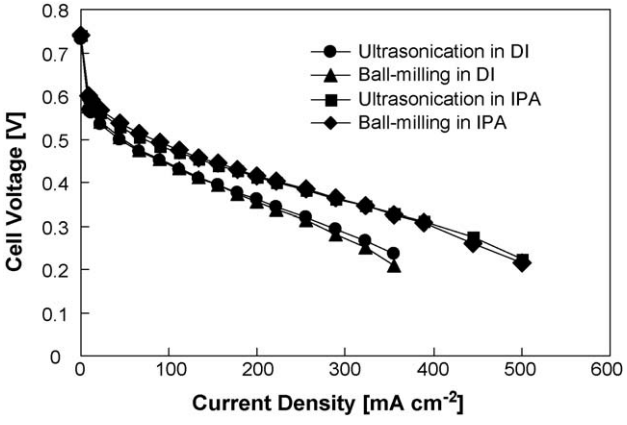

Fig. 7. Polarization curves of MEAs obtained at 90 °C in 1 M CH_3OH and atmospheric pressure air with anodes processed by different catalyst dispersion methods and dispersion media; anode catalyst layer: 2 mg cm^{-2} of Pt-Ru black; cathode catalyst layer: 4.5 mg cm^{-2} of 60 wt.% Pt/C. Anode fuel flow rate was 12 cm^3 min^{-1}, air flow rate 1 dm^3 min^{-1} and active area 9 cm^2.

Even though the activation of the MEA is accelerated by circulating DI through the cathode compartment, in some instances, the cell current of the MEA increased by 20% after 1 week of cell operation due to slow activation of the anode as confirmed by measuring the anode potential with respect to a hydrogen evolving cathode intermittently. Thereafter, it showed a stable value within 5% of current drift for another week of cell operation and is presented in Fig. 8. The MEA with the anode catalyst processed by ball-milling in IPA showed a higher current density in the kinetic-controlled region, from the open circuit potential down to 0.4 V, than that processed by ultrasonication in IPA. On the other hand, in the diffusion-controlled region below 0.35 V, the former showed lower diffusion-limiting currents at both temperatures examined, 60 and 90 °C, than the latter. A brief comparison between the performance results obtained under similar conditions is presented in Table 3.

To examine whether there was a change in catalytic surface area of the anode depending on the type of dispersion method, i.e., ultrasonication and ball-milling, the two anodes were subjected to CO-stripping voltammetry experiments. The results are presented in Fig. 9. The anode processed by ball-milling in IPA exhibited a sharp CO-oxidation peak at 0.343 V_{RHE} while the one processed by ultrasonication in IPA showed a rather broad peak at 0.362 V_{RHE}. It has been known [14] that a higher temperature enhances electrocatalytic activity of Pt-Ru towards oxi-

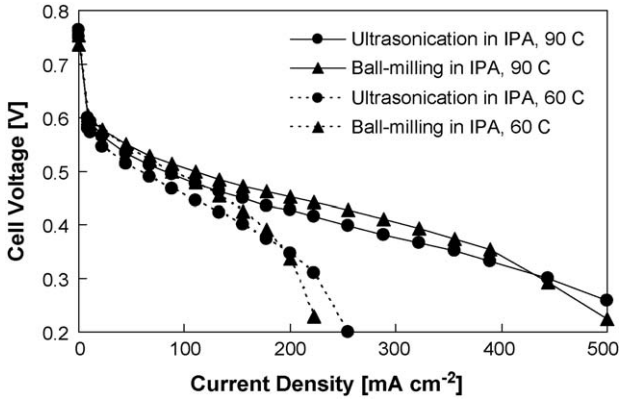

Fig. 8. Polarization curves of MEAs, involving anodes processed by different catalyst dispersion methods in IPA, obtained at 90 °C in 1 M CH_3OH and atmospheric pressure air after 1 week of cell operation; anode catalyst layer: 2 mg cm^{-2} of Pt-Ru black; cathode catalyst layer: 4.5 mg cm^{-2} of 60 wt.% Pt/C.

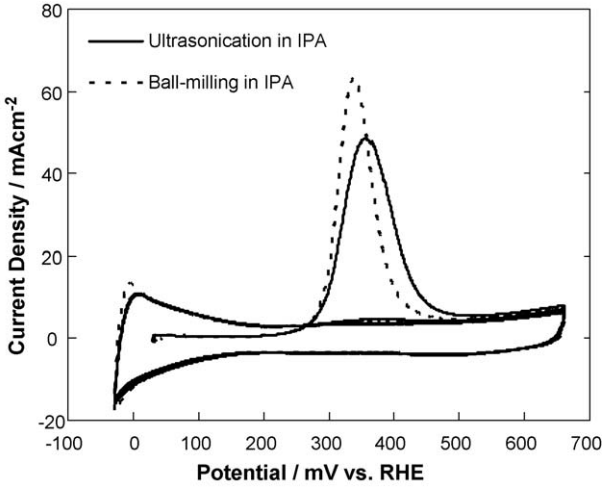

Fig. 9. CO-stripping voltammogram for anodes prepared by two different dispersion methods obtained in 0.5 M H_2SO_4 solution at 60 °C. After a hydration period, CO was adsorbed on the electrode surface at 0.04 V_{RHE} by bubbling CO gas through the electrolyte for 1 h.

dation of adsorbed CO, resulting in lowering the CO-stripping peak potential. In similar experimental condition, they measured the CO-stripping peak potential of the commercial unsupported Pt-Ru black catalyst to be 0.36 V_{RHE} at 60 °C, which is the same value obtained from the ultrasonication-processed anode in this work. McGovern et al. [20] suggested the possibility of the CO-stripping peak shifting to more positive potentials and also a decrease in the CO-stripping peak area due to surface blockage of catalyst particles by the Nafion film. In this work, the peak area for CO-oxidation on the ball-milling processed anode was evaluated to be 766 mC cm^{-2} almost the same as that on the ultrasonication-processed one, resulting in an electrochemical surface area of Pt-Ru catalyst to be 1823 Pt-Ru cm^2 cm^{-2}_{MEA} at 4 mg cm^{-2} of Pt-Ru loading, 191 C $g^{-1}_{Pt\text{-}Ru}$ or 45 m^2 $g^{-1}_{Pt\text{-}Ru}$ based upon a CO-monolayer stripping charge of 420 μC cm^{-2}.

The surface area of unsupported Pt-Ru catalyst (Johnson Matthey, Pt:Ru = 1:1) was estimated to be around 70–78 m^2 $g^{-1}_{Pt\text{-}Ru}$ [14,21], however, it is mentioned [14] that not all of the surface area would be available for methanol electroxidation due to nano-porous structure within catalyst layer and hence approximately only an half of the total surface area would be active for the electrochemical reaction. Considering this fact, the anode fabricated in this study seems to possess high activity toward the electrochemical methanol oxidation. It is noteworthy that the ball-mill-processed anode shows the same CO-stripping peak area as the ultrasonication-processed anode although the ball-mill-processed ink involves bigger catalyst agglomerates than the ultasonication-processed ink does, as shown in Fig. 4(b). Therefore, it is concluded that the better performance of the ball-milling-processed anode is due to a more efficient catalytic reaction toward methanol oxidation than that of the ultrasonication-processed anode, and not due to the catalytic surface area. Since there was no substantial difference in the XRD peak positions, it is believed that the ball-milling process might not induce any significant changes in the composition of the catalyst particles.

As shown in Fig. 6, the catalyst layers appear to be thick enough to consider a morphological effect on the electrochemical oxidation of methanol or carbon monoxide adsorbed on the surface of catalyst. The catalyst layer of the ball-milling processed anode consisting of the flake-shaped catalyst agglomerates in Fig. 6(c) seems to have better connectivity between catalyst particles and simultaneously allow simpler ionic movement of proton in the catalyst layer, leading to a lower electronic ohmic drop through the catalyst layer and a lower ionic ohmic drop through the electrolytic phase inside the pore structure of the catalyst layer, respectively. These factors, in turn, have the effect of increasing the electrocatalytic activity toward methanol oxidation as shown in Fig. 8 and CO-stripping in Fig. 9.

In a simulation study on a fuel cell electrode for DMFC [7], it has been mentioned that carbon dioxide removal from the catalyst layer is particularly important to the methanol fuel cell because high levels of CO_2 can be formed deep inside the cata-

Table 3
Comparison of the power performances obtained under similar conditions using an unsupported Pt-Ru anode catalyst and air

Reference	Current density (A cm^{-2})		Cell temperature (°C)	Oxidant (atm)	MeOH concentration (M)	Anode loading (mg cm^{-2})	Cathode loading (mg cm^{-2})
	at 0.5 V	at 0.4 V					
[4]	0.13	0.31	80	Air 1	1	Pt-Ru 4	Pt 4
[18]	0.12	0.28	80	Air 2	0.5	Pt-Ru 1.3	Pt 1.3
[19]	0.13	0.32	90	Air 2	1	Pt-Ru 3	Pt 3
This work	0.12	0.32	90	Air 1	1	Pt-Ru 2	Pt/C 4.5

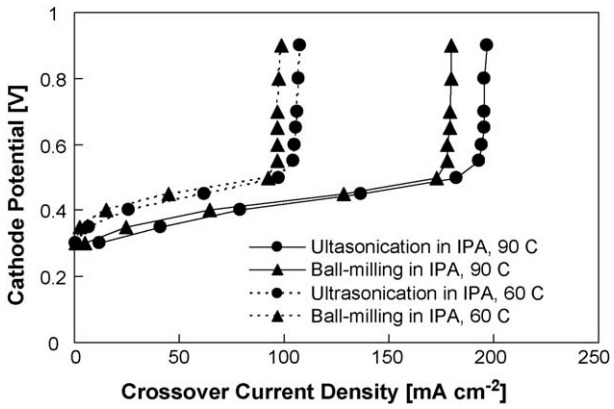

Fig. 10. Open-circuit potential methanol crossover current density measured at cathode by polarizing the cathode anodically in nitrogen atmosphere with respect to an anode in 1 M CH_3OH serving as hydrogen evolving counter electrode.

lyst layer, imposing mass transport limitations on the methanol or the CO_2 via gas bubble formation inside the catalyst layer. Considering the Bruggemann relation [22] in a porous structure:

$$D^{\text{eff}} = D \times \varepsilon^{1.5} \quad (1)$$

where D^{eff} is effective diffusivity and ε porosity, the increased porosity in the anode catalyst layer is expected to facilitate CO_2 removal out of the catalyst layer and hence results in higher diffusion-limiting current at the anode. However, the increase in porosity at a certain amount of catalyst loading inevitably results in an increase in the thickness of catalyst layer and hence a decrease in the diffusion-limiting current. As observed in Fig. 8, the ball-milling processed anode having 25 μm thick catalyst layer represented a lower diffusion-limiting current than the ultrasonication-processed anode having 10–15 μm thick catalyst layer.

As the cathode is subjected to an anodic potential in the nitrogen atmosphere with respect to the anode serving as a hydrogen evolving counter electrode, the anodic current due to methanol crossover through the membrane was recorded as a function of the cathode potential and is presented in Fig. 10. Interestingly, the ball-mill-processed anode represented a lower methanol crossover current than the ultrasonication-processed anode did, due to the thicker catalyst layer which methanol has to pass through prior to crossing the membrane. This result presents that the anode catalyst layer might be able to oxidize the methanol more efficiently as it is fabricated to be more porous and thicker.

4. Conclusions

A new activation procedure, that circulates 1 M aqueous methanol and de-ionized water through the anodic and the cathodic compartment, respectively, at 90 °C at least for 12 h, was successful in ensuring good hydration and hence good reproducibility of the membrane electrode assembly for the direct methanol fuel cell. Independent of the dispersion methods for the anode catalyst layer ink, i.e., an ultrasonication or a ball-milling method, the anode prepared from the ink based on isopropyl alcohol showed a much higher electrochemical activity toward methanol oxidation than the one from the ink based on deionized water. Although XRD patterns from the anodes did not show meaningful differences between the electrodes, the survey of the cross-sectional morphology by SEM on the anode catalyst layers explicitly showed that the anode catalyst layer, fabricated by ball-milling the catalyst in IPA, consisted of flake-shaped agglomerates, exhibiting a higher porosity than the others. The MEA with the anode from the catalyst ink prepared by ball-milling in IPA gave a higher power performance in a kinetic-controlled regime from open-circuit potential to 0.3 V than the MEA with the anode prepared by ultrasonication in the same solvent.

References

[1] X. Ren, M.S. Wilson, S. Gottesfeld, J. Electrochem. Soc. 143 (1996) L12.
[2] M. Baldauf, W. Preidel, J. Power Sources 84 (1999) 161.
[3] A.S. Arico, A.K. Shukla, K.M. el-Khatib, P. Creti, P.L. Antonucci, V. Antonucci, J. Appl. Electrochem. 29 (1999) 671.
[4] B. Gurau, E. Smotkin, J. Power Sources 112 (2002) 339.
[5] A.S. Arico, P.L. Antonucci, E. Modica, V. Baglio, H. Kim, V. Antonucci, Electrochim. Acta 47 (2002) 3723.
[6] C. Lim, C.Y. Wang, J. Power Sources 113 (2003) 145.
[7] J. Wang, R.F. Savinell, Proceedings of the Symposium on Electrode Materials and Processes for Energy Conversion and Storage PV 94-23, The Electrochemical Society Proceedings Series, Pennington, NJ, 1994, p. 326.
[8] Y.H. Chu, Y.G. Shul, W.C. Choi, S.I. Woo, H.S. Han, J. Power Sources 118 (2003) 334.
[9] A. Lindermeir, G. Rosenthal, U. Kunz, U. Hoffmann, J. Power Sources 129 (2004) 180.
[10] J.H. Kim, H.Y. Ha, I.H. Oh, S.A. Hong, H.I. Lee, J. Power Sources 135 (2004) 29.
[11] R.W. Reeve, P.A. Christensen, A.J. Dickinson, A. Hamnett, K. Scott, Electrochim. Acta 45 (2000) 4237.
[12] A.K. Shukla, C.L. Jackson, K. Scott, R.K. Raman, Electrochim. Acta 47 (2002) 3401.
[13] T.A. Zawodzinski Jr., C. Derouin, S. Radzinski, R.J. Sherman, V.T. Smith, T.E. Springer, S. Gottesfeld, J. Electrochem. Soc. 140 (1993) 1041.
[14] H.N. Dinh, X.R. Ren, F.H. Garzon, P. Zelenay, S. Gottesfeld, J. Electroanal. Chem. 491 (2000) 222.
[15] C. He, H.R. Kunz, J.M. Fenton, J. Electrochem. Soc. 150 (2003) A1017.
[16] A.S. Arico, P. Creti, H. Kim, R. Mantegna, N. Giordano, V. Antonucci, J. Electrochem. Soc. 143 (1996) 3950.
[17] M. Uchida, Y. Aoyama, N. Eda, A. Ohta, J. Electrochem. Soc. 142 (1995) 463.
[18] S.C. Thomas, X. Ren, S. Gottesfeld, P. Zelenay, Electrochim. Acta 47 (2002) 3741.
[19] S.Q. Song, Z.X. Liang, W.J. Zhou, G.Q. Sun, Q. Xin, V. Stergiopoulos, P. Tsiakaras, J. Power Sources 145 (2005) 495.
[20] M.S. McGovern, E.C. Garnett, C. Rice, R.I. Masel, A. Wieckowski, J. Power Sources 115 (2003) 35.
[21] S.T. Kuk, A. Wieckowski, J. Power Sources 141 (2005) 1.
[22] R.E. De la Rue, C.W. Tobias, J. Electrochem. Soc. 106 (1959) 827.